



## Strathprints Institutional Repository

**You, Tao and Yue, Hong (2015) Investigating receptor enzyme activity using time-scale analysis. IET Systems Biology, 9 (6). pp. 268-276. ISSN 1751-8849 , <http://dx.doi.org/10.1049/iet-syb.2015.0037>**

This version is available at <http://strathprints.strath.ac.uk/55252/>

**Strathprints** is designed to allow users to access the research output of the University of Strathclyde. Unless otherwise explicitly stated on the manuscript, Copyright © and Moral Rights for the papers on this site are retained by the individual authors and/or other copyright owners. Please check the manuscript for details of any other licences that may have been applied. You may not engage in further distribution of the material for any profitmaking activities or any commercial gain. You may freely distribute both the url (<http://strathprints.strath.ac.uk/>) and the content of this paper for research or private study, educational, or not-for-profit purposes without prior permission or charge.

Any correspondence concerning this service should be sent to Strathprints administrator: [strathprints@strath.ac.uk](mailto:strathprints@strath.ac.uk)

# Investigating receptor enzyme activity using time scale analysis

Tao You<sup>1</sup>, Hong Yue<sup>2</sup>

<sup>1</sup>Computational Biology, Discovery Sciences, Innovative Medicines & Early Development,  
AstraZeneca, Alderley Park, Cheshire, SK10 4TG, UK. Email: dr.tao.you@gmail.com

<sup>2</sup>Department of Electrical and Electronic Engineering, University of Strathclyde, Glasgow,  
G1 1XW, UK. Email: hong.yue@strath.ac.uk

---

## Abstract

At early drug discovery, purified protein-based assays are often used to characterize compound potency. In the context of dose response, it is often perceived that a time-independent inhibitor is reversible and a time-dependent inhibitor is irreversible. The legitimacy of this argument is investigated using a simple kinetics model, where it is revealed by model-based analytical analysis and numerical studies that dose response of an irreversible inhibitor may appear time-independent under certain parametric conditions. Hence, the observation of time-independence cannot be used as sole evidence for identification of inhibitor reversibility. It has also been discussed how the synthesis and degradation of a target receptor affect drug inhibition in an in vitro cell-based assay setting. These processes may also influence dose response of an irreversible inhibitor in such a way that it appears time-independent under certain conditions. Furthermore, model-based steady-state analysis reveals the complexity nature of the drug-receptor process.

## Keywords

Inhibitor reversibility; receptor turnover; mathematical modelling; dose response; time-scale analysis

---

## 29 **1 Introduction**

30 Drug discovery and development typically involve protein-based studies (e.g. target  
31 engagement; typical time scale: microseconds to minutes), in vitro cell-based studies (e.g.  
32 biomarker pharmacodynamics (PD), therapeutic efficacy; typical time scale: minutes to days),  
33 in vivo animal-based studies (e.g. pharmacokinetics (PK), biomarker PD, therapeutic efficacy,  
34 safety evaluation; typical time scale: hours to days) and clinical trials (e.g. PK, PD, safety,  
35 efficacy; typical time scale: days to months). These studies are often organized in this  
36 particular temporal order, in the hope that the results of a previous step (e.g. protein-based  
37 assay) will help inform the design and interpretation of the subsequent experiment (e.g. in  
38 vitro cell assay).

39 A new paradigm that helps enable robust translation of each type of study arises in recent  
40 years [1], in which mathematical models and model-based systems analysis have played  
41 increasingly important roles. Model development of drug processes using experimental data  
42 has been largely improved through various efforts including sensitivity analysis, parameter  
43 identifiability analysis, model approximation and simplification, model validation and  
44 comparison, etc. [2-5].

45 Known as Quantitative & Systems Pharmacology (QSP), it employs multi-scale  
46 modelling approaches to integrate data generated from different studies in a drug discovery  
47 and development programme, which span different temporal and dimensional scales [6-8].  
48 These computational models are able to reconcile different experimental conditions (e.g. in  
49 vitro cell assays and in vivo animal models [9]), with an ultimate aim of bridging preclinical  
50 models to an appropriate clinical setting, and generating statistically robust predictions that  
51 are validated by preclinical and clinical data [10].

52 Multi-scale modelling has been successfully deployed in drug development programmes,  
53 so that in vitro cell-based studies are consistently integrated with in vivo animal-based studies.  
54 However, the application of QSP approaches in early drug discovery (i.e. integration of  
55 results from protein-based studies and in vitro cell-based studies) has been relatively limited  
56 [11]. QSP models are urgently needed to better understand target engagement in cell-free  
57 environment and in cells, so as to help design of subsequent in vitro and in vivo studies [1].

58 It is often important to establish dose–response relationship specific for an inhibitor and a  
59 cell type under investigation, which describes the change in effect on a cell caused by  
60 differing levels of exposure (or doses) to an inhibitor after a certain exposure time.

61 To help translate in vitro results into in vivo knowledge, models of Target Mediated Drug  
62 Disposition (TMDD) have been developed to analyse receptor PK/PD relationships [2-5; 7; 8;  
63 12-15]. In addition to drug binding and receptor turnover, these models also consider the  
64 elimination of all species, to mimic in vivo conditions. They can be served as a useful  
65 theoretical framework. Model-based analysis revealed that the necessary and sufficient  
66 condition for receptor rebound in a single dose animal experiment is that elimination rate of  
67 the drug-receptor product being slower than the elimination rates of the drug and of the  
68 receptor [12]. Under the assumption of a constant target pool, the characteristic features of  
69 TMDD dynamics were studied through a mathematical model analysis [13]. A time-scale  
70 analysis was performed to provide accurate approximations of the temporal evolution under  
71 the assumption of high drug binding affinity [14].

72 Although TMDD models have been used increasingly to facilitate PK/PD studies, cellular  
73 kinetics may sometimes not be fully appreciated in design of protein-based assays. For  
74 instance, the potency of a chemical entity to inhibit an enzyme is often characterized by  $IC_{50}$ ,  
75 the chemical concentration that generates half of maximal inhibition. For an irreversible  
76 inhibitor that covalently modifies a purified target enzyme in a cell-free assay, the chemical  
77 reaction tends to be more complete given a longer drug incubation period. Consequently,  $IC_{50}$   
78 usually exhibits incubation time-dependent shift, making the inhibitor appear more potent at  
79 long incubation periods [16-18]. In contrast, a target protein in a living cell undergoes  
80 turnover (i.e. synthesis and degradation) that are often regulated via transcriptional regulation,  
81 translational control [19] and cell signalling etc. These processes typically happen within  
82 minutes to hours [20], and they may influence cellular response to drug inhibition. In other  
83 words, shooting a moving target in a cell might be different from shooting an immobile target  
84 in a protein-based assay.

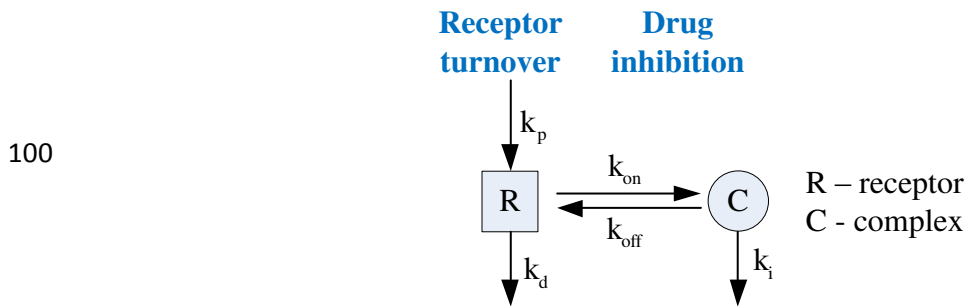
85 The aim of this study is to investigate how drug parameters and cell parameters influence  
86 cellular response to drug treatment at constant drug concentration. We are interested in  
87 understanding whether an irreversible inhibitor necessarily has an incubation time-dependent  
88  $IC_{50}$  in a protein-based study. In addition, we hope to examine how cell parameters including  
89 target synthesis and degradation rates affect dose response.

90 The remaining of the paper is organized as follows. A linear model of receptor turnover  
91 and irreversible inhibition is proposed and discussed in Section 2. Investigation of fast drug  
92 process relative to receptor turnover is discussed in Section 3, where both numerical  
93 simulation and ensuing analysis of the eigenvalues are employed. Discussions on slow drug

94 process relative to receptor turnover are presented in Section 4. In Section 5, an application of  
 95 this model is attempted using aberrant activity in Epidermal Growth Factor Receptor (EGFR)  
 96 signaling data. Conclusions are given in Section 6.

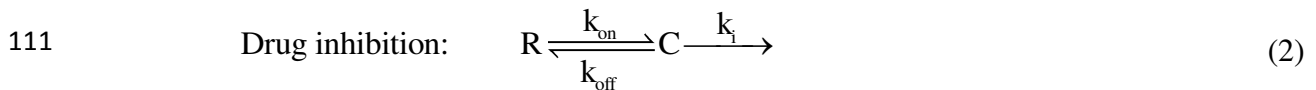
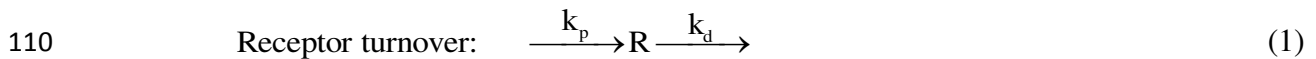
97 **2 A model of receptor turnover and drug inhibition**

98 A simple model is proposed to recapitulate the process of receptor turnover, i.e. receptor  
 99 synthesis and degradation, together with drug inhibition as shown schematically in Fig. 1.



101 **Fig. 1** Schematic description of receptor turnover and irreversible inhibition

102 In the receptor turnover process, receptor R is synthesized at a constant rate  $k_p$ , and degrades  
 103 following a first-order kinetics with a rate constant  $k_d$ . For the sake of simplicity, feedback  
 104 mechanisms and subcellular localisation that regulate protein synthesis and stability are not  
 105 considered in this model. In the drug inhibition process, a drug molecule first binds R  
 106 reversibly to comprise an intermediate complex C with association and dissociation rates  $k_{on}$   
 107 and  $k_{off}$ , respectively. Note that  $k_{on}$  is an apparent rate that depends on drug concentration.  
 108 The complex C then forms a covalent bound irreversibly at the second step, in a first-order  
 109 reaction with a rate constant  $k_i$ . These two processes can be described respectively as follows.



112 Based on mass-balance principles, the corresponding ordinary differential equations (ODEs)  
 113 for concentrations of R and C, denoted as R and C, respectively, are written as

114 
$$\frac{dR}{dt} = -(k_d + k_{on})R + k_p + k_{off}C \quad (3)$$

115 
$$\frac{dC}{dt} = k_{on}R - (k_{off} + k_i)C \quad (4)$$

116 with the following units: nM for R, C; nM·min<sup>-1</sup> for k<sub>p</sub>; and min<sup>-1</sup> for k<sub>d</sub>, k<sub>on</sub>, k<sub>off</sub> and k<sub>i</sub>.  
 117 Here k<sub>p</sub> and k<sub>d</sub> are cell parameters associated to receptor turnover; k<sub>on</sub>, k<sub>off</sub> and k<sub>i</sub> are drug  
 118 parameters for covalent inhibition process.

119 In the absence of drug, the receptor has a steady state at R<sub>0</sub> = k<sub>p</sub>/k<sub>d</sub> nM. Scaling R and C  
 120 with R<sub>0</sub> in (3) and (4), the two concentration variables become dimensionless terms  
 121 r = R/R<sub>0</sub> = Rk<sub>d</sub>/k<sub>p</sub> and c = C/R<sub>0</sub> = Ck<sub>d</sub>/k<sub>p</sub>, respectively, and the ODE model can then be  
 122 written as

123 
$$\frac{dr}{dt} = -(k_d + k_{on})r + k_d + k_{off}c \quad (5)$$

124 
$$\frac{dc}{dt} = k_{on}r - (k_{off} + k_i)c \quad (6)$$

125 In this dimension-free representation, the initial conditions are set to be r<sub>0</sub> = r(0) = 1 and  
 126 c<sub>0</sub> = c(0) = 0. We further use k<sub>off</sub> to scale the time term by τ = k<sub>off</sub>t, and also to scale  
 127 reaction rates with κ<sub>on</sub> = k<sub>on</sub>/k<sub>off</sub>, κ<sub>i</sub> = k<sub>i</sub>/k<sub>off</sub>, and κ<sub>d</sub> = k<sub>d</sub>/k<sub>off</sub>. This brings the following  
 128 two ODEs for dimensionless r and c, respectively:

129 
$$\frac{dr}{d\tau} = -(\kappa_{on} + \kappa_d)r + c + \kappa_d \quad (7)$$

130 
$$\frac{dc}{d\tau} = \kappa_{on}r - (1 + \kappa_i)c \quad (8)$$

131 Denoting  $\mathbf{X} = [r \ c]^T$ , this ODE model can be written in a matrix format

132 
$$\begin{aligned} \dot{\mathbf{X}} &= \begin{bmatrix} \dot{r} \\ \dot{c} \end{bmatrix} = \begin{bmatrix} \frac{dr}{d\tau} \\ \frac{dc}{d\tau} \end{bmatrix} = \begin{bmatrix} -(\kappa_{on} + \kappa_d) & 1 \\ \kappa_{on} & -(1 + \kappa_i) \end{bmatrix} \begin{bmatrix} r \\ c \end{bmatrix} + \begin{bmatrix} \kappa_d \\ 0 \end{bmatrix} \\ &= \mathbf{AX} + \mathbf{f} \quad \text{with} \quad \mathbf{X}(0) = \mathbf{X}_0 \end{aligned} \quad (9)$$

133 where  $\mathbf{A} = \begin{bmatrix} -(\kappa_{\text{on}} + \kappa_{\text{d}}) & 1 \\ \kappa_{\text{on}} & -(1 + \kappa_{\text{i}}) \end{bmatrix}$  is the state matrix for this linear-time-invariant (LTI)  
 134 system;  $\mathbf{f} = [\kappa_{\text{d}} \ 0]^T$  is the nonhomogeneous part;  $\mathbf{X}_0 = [1 \ 0]^T$  is the vector of initial states  
 135 for  $\mathbf{X}$ .

136 At the steady state when  $dr/d\tau = 0$  and  $dc/d\tau = 0$ , the steady-state values for  $r$  and  $c$  are  
 137 derived from (9) to give

$$138 \quad r_{\text{ss}} = \frac{(1 + \kappa_{\text{i}})\kappa_{\text{d}}}{(1 + \kappa_{\text{i}})\kappa_{\text{d}} + \kappa_{\text{on}}\kappa_{\text{i}}} \quad (10)$$

$$139 \quad c_{\text{ss}} = \frac{\kappa_{\text{on}}\kappa_{\text{d}}}{(1 + \kappa_{\text{i}})\kappa_{\text{d}} + \kappa_{\text{on}}\kappa_{\text{i}}} \quad (11)$$

140 Here  $r_{\text{ss}}$  and  $c_{\text{ss}}$  are used to denote steady-state values or equilibrium points for  $r$  and  $c$ ,  
 141 respectively, when time approaches infinity.

142 Note after the above re-scaling, all terms in (9) are dimensionless including concentration  
 143 variables  $r$  and  $c$ ; time  $\tau$ ; and parameters  $\kappa_{\text{on}}$ ,  $\kappa_{\text{i}}$ , and  $\kappa_{\text{d}}$ . The ‘disappeared’ receptor  
 144 synthesis rate  $k_{\text{p}}$  is included in  $\kappa_{\text{d}}$  through scaling of  $\kappa_{\text{d}} = k_{\text{d}}/k_{\text{off}} = k_{\text{p}}/(k_{\text{off}}R_0)$ . Clearly this  
 145 choice of non-dimensionalization requires that  $k_{\text{off}} \neq 0$  and  $k_{\text{p}} \neq 0$ . All variables and  
 146 parameters in (9) are associated with physical quantities and therefore must be nonnegative.  
 147 With this dimensionless model, the analysis of system behaviour under different parametric  
 148 regimes can be conveniently discussed in a unified scheme.

### 149 **3 Fast drug process relative to receptor turnover**

150 The parametric regimes have been divided into that of fast drug process and slow drug  
 151 process. In this section, the process of fast drug binding and dissociation is firstly discussed.

#### 152 **3.1 Fast drug binding and dissociation relative to receptor turnover**

153 This parametric regime is defined by  $k_{\text{off}} \gg k_{\text{d}}$  and  $k_{\text{on}} \gg k_{\text{d}}$ . In this case, the receptor  
 154 turnover rate  $k_{\text{d}}$  is much smaller than the drug binding and dissociation rates  $k_{\text{on}}$  and  $k_{\text{off}}$ .

- 155 (a) When  $k_{\text{off}} \gg k_d$ , i.e.,  $\kappa_d \ll 1$ , the period of target coverage (characterized by  $1/k_{\text{off}}$ )  
 156 is much shorter than that of receptor degradation (characterized by  $1/k_d$ ), which can  
 157 be due to: i) short target coverage; ii) slow receptor degradation; and iii) combination  
 158 of i) and ii).
- 159 (b) When  $k_{\text{on}} \gg k_d$ , i.e.,  $\kappa_{\text{on}} \gg \kappa_d$ , a receptor binds a drug molecule at a rate much faster  
 160 than its degradation.

161 Under these two conditions, the term of  $\kappa_d$  can be ignored, and model (9) is approximated by

$$162 \quad \begin{bmatrix} \dot{r} \\ \dot{c} \end{bmatrix} = \begin{bmatrix} -\kappa_{\text{on}} & 1 \\ \kappa_{\text{on}} & -(1 + \kappa_i) \end{bmatrix} \begin{bmatrix} r \\ c \end{bmatrix} \quad (12)$$

163 Model (12) is actually an ODE model for the cell-free assay with only the drug process in (2)  
 164 considered.

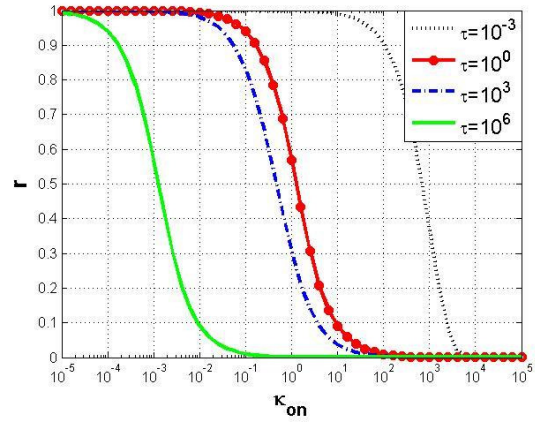
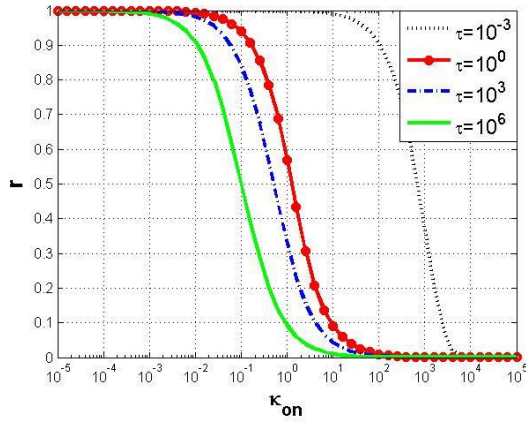
165 When  $\kappa_i \neq 0$ , by taking  $dr/d\tau = 0$  and  $dc/d\tau = 0$ , the steady-state of dynamic system  
 166 (12) is deduced to be

$$167 \quad r_{\text{ss}} = c_{\text{ss}} = 0 \quad (13)$$

168 How small does  $k_d$  have to be in comparison to  $k_{\text{off}}$  and  $k_{\text{on}}$  so as to ensure the validity  
 169 of this approximation? This is examined by the following numerical simulation. Firstly, the  
 170 full model in (9) is simulated with  $\kappa_i = 0.001$  ( $k_{\text{off}} \gg k_i$ ) at three different levels of  $\kappa_d$ :  
 171  $\kappa_d = 10^{-4}$  (Fig. 2 (a));  $\kappa_d = 10^{-6}$  (Fig. 2 (b)); and  $\kappa_d = 10^{-8}$  (Fig. 2 (c)). Then the full model is  
 172 simulated by taking  $\kappa_d = 0$ , which is equivalent to the reduced model in (12), using identical  
 173 value for  $\kappa_i$ , as shown in Fig. 2 (d). The range of  $\kappa_{\text{on}}$  is set to be  $[1e-5, 1e5]$  in all  
 174 simulations. Four incubation time periods are chosen which are separated with an order of 3  
 175 in time scale between each two, i.e.,  $10^{-3}$ , 1,  $10^3$  and  $10^6$ . Comparing simulation results across  
 176 the four panels in the semi-log Fig. 2, it can be observed that there is a clear difference in  
 177 dose response in both Fig. 2 (a) and Fig. 2 (b) when compared with the simplified model  
 178 results in Fig. 2 (d), but the dose response in Fig. 2 (c) is almost the same as that in Fig. 2 (d).  
 179 This shows that, when  $\kappa_d \leq 10^{-8}$ , model (12) provides a close approximation for dose  
 180 responses corresponding to incubation time up to  $10^6$ .



181 In all simulation and illustrative results in this paper, the time terms are represented in  $\tau$   
 182 (time  $t$  scaled by  $k_{\text{off}}$ ), and the x-axis for  $\kappa_{\text{on}}$  is in  $\log_{10}$  scale in dose-response curves.

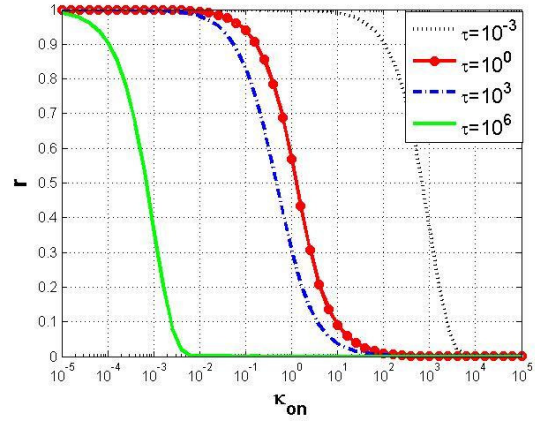
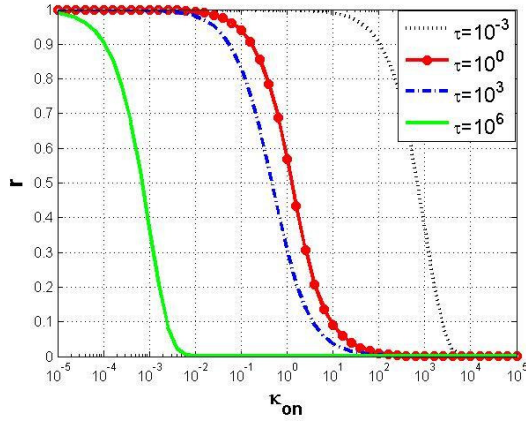


183

184

(a) Full model at  $\kappa_d = 10^{-4}$

(b) Full model at  $\kappa_d = 10^{-6}$



185

186

(c) Full model at  $\kappa_d = 10^{-8}$

(d) Simplified model (12)

187 **Fig. 2** Dose response curves predicted for four different incubation times, when  $\kappa_i = 0.001$ .  
 188 Incubation times shown in the figure legend: black dotted line for  $10^{-3}$ ; red line with circles  
 189 for  $10^0$ ; blue dash-dot line for  $10^3$ ; green solid line for  $10^6$ . (a) Full model (9) simulated at  
 190  $\kappa_d = 10^{-4}$ ; (b) Full model simulated at  $\kappa_d = 10^{-6}$ ; (c) Full model simulated at  $\kappa_d = 10^{-8}$ ; (d)  
 191 Approximate model in (12).

192 The approximate model in (12) represents a homogeneous LTI system with

193 
$$\mathbf{A} = \begin{bmatrix} -\kappa_{\text{on}} & 1 \\ \kappa_{\text{on}} & -(1 + \kappa_i) \end{bmatrix}$$
. We can use the eigenvalue method to analyse its dynamic

194 characteristics. Denoting the trace and determinant of matrix  $\mathbf{A}$  as

195  $T = \text{trace}(\mathbf{A}) = -(1 + \kappa_{\text{on}} + \kappa_i)$ ,  $\Delta = \det(\mathbf{A}) = \kappa_{\text{on}} \cdot \kappa_i$ , the eigenvalues of  $\mathbf{A}$  are calculated by

196 
$$\lambda_{1,2} = \left( T \mp \sqrt{T^2 - 4\Delta} \right) / 2.$$

197 For the first eigenvalue

198 
$$\lambda_1 = -\frac{1}{2}(1 + \kappa_{\text{on}} + \kappa_i) - \frac{1}{2}\sqrt{(1 + \kappa_{\text{on}} + \kappa_i)^2 - 4\kappa_{\text{on}}\kappa_i}, \quad (14)$$

199 its associated eigenvector is

200 
$$\mathbf{v}_1 = [v_{11} \quad v_{21}]^T = \left[ \begin{array}{c} \frac{1 + \kappa_i - \kappa_{\text{on}} - \sqrt{(1 + \kappa_{\text{on}} + \kappa_i)^2 - 4\kappa_{\text{on}}\kappa_i}}{2\kappa_{\text{on}}} \\ 1 \end{array} \right]^T. \quad (15)$$

201 For the second eigenvalue

202 
$$\lambda_2 = -\frac{1}{2}(1 + \kappa_{\text{on}} + \kappa_i) + \frac{1}{2}\sqrt{(1 + \kappa_{\text{on}} + \kappa_i)^2 - 4\kappa_{\text{on}}\kappa_i}, \quad (16)$$

203 its associated eigenvector is

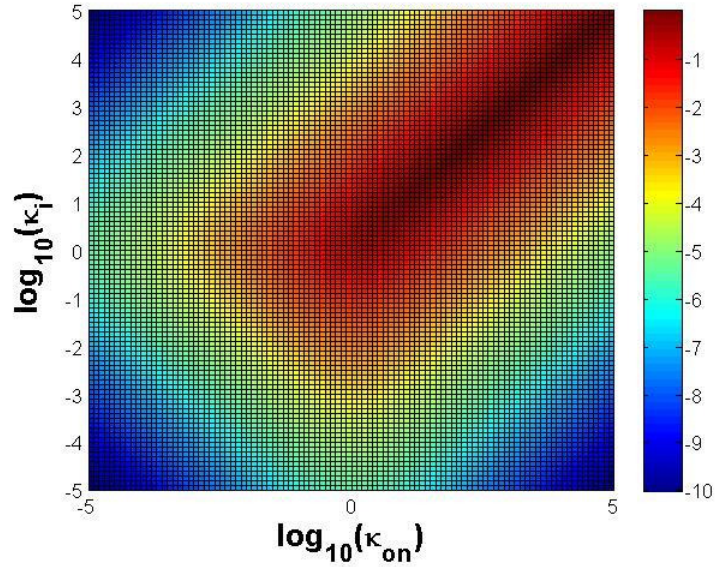
204 
$$\mathbf{v}_2 = [v_{12} \quad v_{22}]^T = \left[ \begin{array}{c} \frac{1 + \kappa_i - \kappa_{\text{on}} + \sqrt{(1 + \kappa_{\text{on}} + \kappa_i)^2 - 4\kappa_{\text{on}}\kappa_i}}{2\kappa_{\text{on}}} \\ 1 \end{array} \right]^T. \quad (17)$$

205 With initial conditions  $r_0 = 1$  and  $c_0 = 0$ , a general analytical solution for (12) can be  
206 succinctly written as

207 
$$\mathbf{M}(\tau) = \begin{bmatrix} r(\tau) \\ c(\tau) \end{bmatrix} = \frac{1}{v_{11} - v_{12}} \begin{bmatrix} v_{11}e^{\lambda_1\tau} - v_{12}e^{\lambda_2\tau} \\ e^{\lambda_1\tau} - e^{\lambda_2\tau} \end{bmatrix} \quad (18)$$

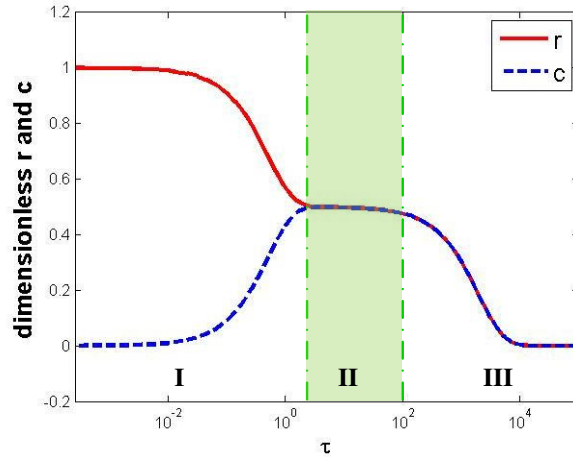
208 where all terms regarding eigenvalues and entries in eigenvectors are provided in (14) - (17).

209 The  $\log_{10}$  transformed ratio of the two eigenvalues for different pairs of  $(\kappa_{\text{on}}, \kappa_i)$  is  
210 plotted in a heat map as shown in Fig. 3. From this diagram it is evident that when the two  
211 parameters have similar values and are both above 1, the two eigenvalues  $\lambda_1$  and  $\lambda_2$  are close  
212 to each other (the red area in Fig. 3). However, if only one parameter is much larger than 1 or  
213 both parameters are much smaller than 1, then the two eigenvalues are widely apart from  
214 each other, i.e.  $\lambda_2 / \lambda_1 \ll 1$  (the blue area in Fig. 3), and the time response of the system is  
215 mainly determined by  $|\lambda_1|$  in a shorter period.



216

217 **Fig. 3**  $\log_{10}(\lambda_2 / \lambda_1)$  plotted as a function of  $\log_{10}(\kappa_{\text{on}})$  and  $\log_{10}(\kappa_i)$ . Values between -10  
 218 and 0 are colour-coded.



219

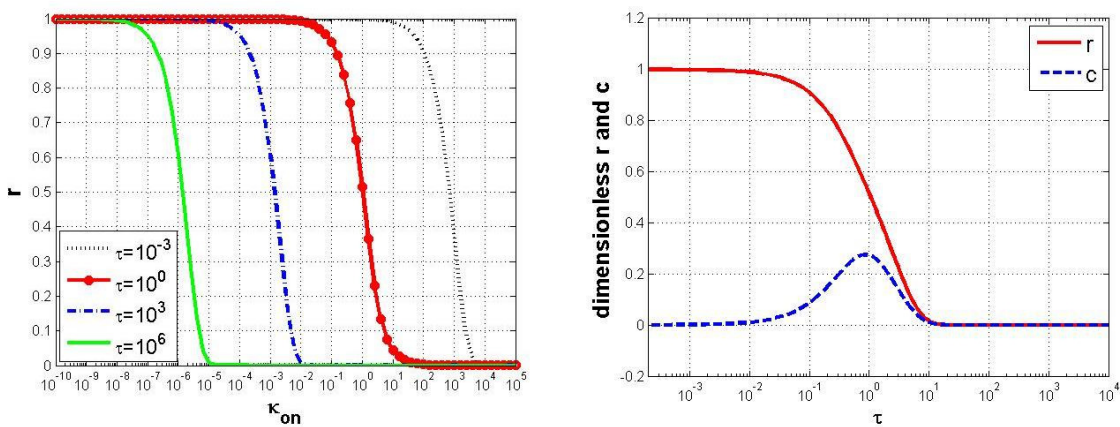
220 **Fig. 4** Time responses of  $r$  and  $c$  under  $\kappa_{\text{on}} = 1$ ,  $\kappa_i = 0.001$  and  $\kappa_d = 0$ .

221 For example, when  $\kappa_{\text{on}} = 1$ ,  $\kappa_i = 0.001$ , from (14) to (17), the eigenvalues and  
 222 eigenvectors can be calculated as:  $\lambda_1 = -2.005$ ,  $\lambda_2 = -5 \times 10^{-4}$ ,  $\mathbf{v}_1 = [-0.7069 \ 0.7069]^T$  and  
 223  $\mathbf{v}_2 = [-0.7073 \ -0.7069]^T$ . The short-term time response is driven by  $|\lambda_1|$  (see region I in Fig.  
 224 4), and the long-term time response is driven by  $|\lambda_2|$  (see region III in Fig. 4). Interestingly,  
 225 between these two regions, both  $r$  and  $c$  have relatively small variations (see region II in Fig.  
 226 4). Hence, corresponding dose responses simulated for observation times in this shadowed  
 227 region would appear to be similar using experimental data. This time-independent  
 228 observation may suggest a reversible inhibition, which is not true from the above analysis.

229 3.2 Fast drug binding/dissociation and fast covalent modification

230 The parametric regime for this scenario is classified by:  $\kappa_{\text{on}} \gg \kappa_{\text{d}}$ ,  $\kappa_{\text{off}} \gg \kappa_{\text{d}}$ , and  
 231  $\kappa_{\text{i}} \approx \kappa_{\text{on}}$ , therefore  $\kappa_{\text{i}} \gg \kappa_{\text{d}}$ . In this case, both reversible binding/dissociation and irreversible  
 232 modification are much faster than receptor turnover. The system can also be modelled by (12).  
 233 It can be seen from the heat map in Fig. 3 that the two eigenvalues are close to each other in  
 234 this region, which means the two inherent time scales are not far away from each other. For  
 235 the simulations demonstrated in Fig. 5, the two eigenvalues are  $\lambda_1 = -2.618$  and  $\lambda_2 = -0.382$ ,  
 236 calculated from (14) and (16), respectively. In this case, the dose response curves measured at  
 237 different incubation times are predicted to be clearly separated from each other (Fig. 5 (a)).

238 The concentrations of R and C reach steady states with both values at 0 (Fig. 5 (b)), which  
 239 is consistent with the steady-state analysis conclusion given in (13). Similar to the simulation  
 240 results shown in Fig. 4, Fig. 5 (b) also demonstrates that the receptor concentration decreases  
 241 monotonically to its steady state, but the complex concentration goes through a rapid increase  
 242 initially and then decreases in a slower time scale to its steady state.



243 (a) Dose response curves

(b) Time responses under  $\kappa_{\text{on}} = 1$

245 **Fig. 5** Dose response curves and time responses of  $r$  and  $c$  under  $\kappa_{\text{d}} = 0$ ,  $\kappa_{\text{on}} = \kappa_{\text{i}} = 1$ .

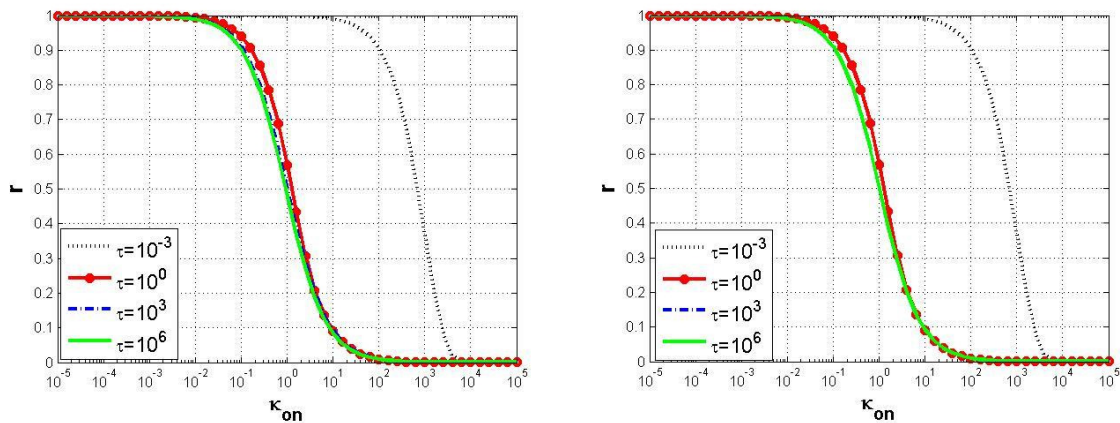
246 3.3 Fast drug binding/dissociation and slow covalent modification

247 Under the condition of fast drug process over receptor turnover ( $k_{\text{off}} \gg k_{\text{d}}$  and  $k_{\text{on}} \gg k_{\text{d}}$ ),  
 248 we further consider the regime of  $k_{\text{off}} \gg k_{\text{i}}$ , i.e.,  $\kappa_{\text{i}} \ll 1$ . This means the drug dissociation is  
 249 much faster than the covalent modification. It corresponds to the region in lower part of the  
 250 heat map in Fig. 3. This condition is satisfied if i) an irreversible inhibitor has to overcome a

251 relatively large energy barrier to covalently modify the receptor; ii) drug dissociation is rapid;  
 252 iii) a combination of both. Within the parametric region of  $\kappa_{\text{on}} \gg \kappa_{\text{d}}$ ,  $\kappa_{\text{d}} \ll 1$  and  $\kappa_{\text{i}} \ll 1$ ,  
 253 model (12) can be further reduced to

$$254 \quad \begin{bmatrix} \dot{r} \\ \dot{c} \end{bmatrix} = \begin{bmatrix} -\kappa_{\text{on}} & 1 \\ \kappa_{\text{on}} & -1 \end{bmatrix} \begin{bmatrix} r \\ c \end{bmatrix} \quad (19)$$

255 Model (19) is a description for protein-based assay when reversible inhibitor is applied  
 256 while the covalent modification is negligible. In order to determine how small  $\kappa_{\text{i}}$  should be  
 257 so that the simplified model in (19) can be applied, simulations are conducted using the full  
 258 model under  $\kappa_{\text{d}} = 10^{-8}$ , and reduce  $\kappa_{\text{i}}$  gradually to search for the threshold level that will  
 259 produce a response close to the simplified model response. Fig. 6 shows that when  $\kappa_{\text{i}}$  is  
 260 reduced to  $1 \times 10^{-7}$ , the full-model response is very close to that of the simplified model (19).  
 261 This suggests that when  $\kappa_{\text{i}} \leq 10^{-7}$ , the simplified model in (19) can be used to approximate  
 262 model (12) with a good accuracy.



263 (a) Full model at  $\kappa_{\text{d}} = 1 \times 10^{-8}$ ,  $\kappa_{\text{i}} = 1 \times 10^{-7}$  (b) Approximate model (19)

265 **Fig. 6** Dose response curves predicted for different incubation times in  $\tau$ : black dotted line  
 266 for  $10^{-3}$ ; red line with circles for  $10^0$ ; blue dash-dot line for  $10^3$ ; green solid line for  $10^6$ . (a)  
 267 Full model (9) simulated at  $\kappa_{\text{d}} = 1 \times 10^{-8}$ ,  $\kappa_{\text{i}} = 1 \times 10^{-7}$ ; (b) Approximate model in (19).

268 In this case,  $\frac{dr}{d\tau} = -\frac{dc}{d\tau}$ ,  $T = \text{trace}(\mathbf{A}) = -(1 + \kappa_{\text{on}})$ ,  $\Delta = \det(\mathbf{A}) = 0$ ,  $\lambda_1 = T = -(\kappa_{\text{on}} + 1)$  and  
 269  $\lambda_2 = 0$ . Under the given initial conditions, the time responses of the two dimensionless  
 270 concentration terms can be solved explicitly to yield

271

$$r(\tau) = \frac{1}{1 + \kappa_{\text{on}}} \left( 1 + \kappa_{\text{on}} e^{-(1+\kappa_{\text{on}})\tau} \right) \quad (20)$$

$$c(\tau) = \frac{\kappa_{\text{on}}}{1 + \kappa_{\text{on}}} \left( 1 - e^{-(1+\kappa_{\text{on}})\tau} \right)$$

272 The time scale of this dynamic system is determined by  $|\lambda_1|$  or by  $\kappa_{\text{on}}$ . The larger is  $\kappa_{\text{on}}$ , the  
 273 faster response the system has, and vice versa. The time responses of  $r$  and  $c$  under different  
 274 levels of  $\kappa_{\text{on}}$  are illustrated in Fig. 7.

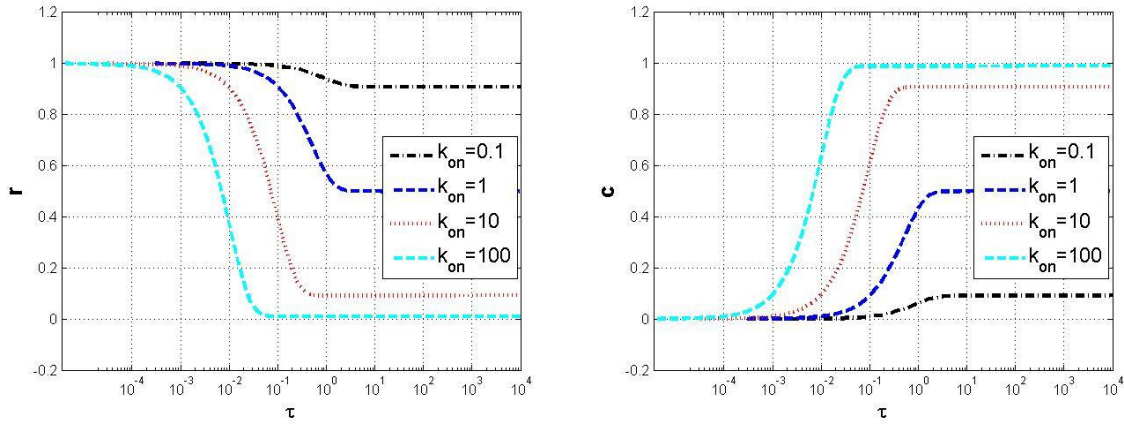
275 With model (19), the steady state is not determined by (13) since  $\kappa_i$  is taken to be zero. In  
 276 fact, the equilibrium points for system (19) can be derived from (20) to give

277

$$r_{\text{ss}} = \lim_{\tau \rightarrow \infty} \frac{1}{1 + \kappa_{\text{on}}} \left( 1 + \kappa_{\text{on}} e^{-(1+\kappa_{\text{on}})\tau} \right) = \frac{1}{1 + \kappa_{\text{on}}} \quad (21)$$

$$c_{\text{ss}} = \lim_{\tau \rightarrow \infty} \frac{\kappa_{\text{on}}}{1 + \kappa_{\text{on}}} \left( 1 - e^{-(1+\kappa_{\text{on}})\tau} \right) = \frac{\kappa_{\text{on}}}{1 + \kappa_{\text{on}}}$$

278 It can be concluded that  $r_{\text{ss}} + c_{\text{ss}} = 1$  at the steady state. The larger is  $\kappa_{\text{on}}$ , the smaller is  $r_{\text{ss}}$   
 279 and the larger is  $c_{\text{ss}}$ . This can be clearly seen in the dynamic simulation results shown in Fig.  
 280 7.



281

(a) Time response  $r$

(b) Time response  $c$

283 **Fig. 7** Time responses of  $r$  and  $c$  with approximate model (19) under different levels of  $\kappa_{\text{on}}$ .

284 For incubation time  $\tau_m \gg 1/(1 + \kappa_{\text{on}})$ ,  $r$  is close to its steady state (see simulation for each  
 285  $\kappa_{\text{on}}$  in Fig. 7). Hence, dose response measurements taken beyond this point would appear  
 286 time-invariant.



287 In summary, our analysis of fast drug process suggests for dose response to appear time-  
 288 invariant, the following two requirements need to be satisfied. Firstly, the apparent first-order  
 289 rate  $\kappa_{\text{on}}$  and the first-order covalent bond formation rate  $\kappa_i$  need to be largely different so  
 290 that the two time scales characterized by  $1/|\lambda_1|$  and  $1/|\lambda_2|$  are well separated from each other.  
 291 Secondly, observation time has to be between the two time scales, which corresponds to  
 292 region II in Fig. 4. It can also be observed from dynamic study that the receptor concentration  
 293 always decreases monotonically to a steady-state level of zero for the fast drug process, while  
 294 the concentration of complex C increases rapidly first and then decreases gradually to zero  
 295 except for the case when covalent modification to complex C is negligible, i.e.  $\kappa_i = 0$ .

#### 296 4 Slow drug process relative to receptor turnover

297 In the parametric regime where  $k_{\text{off}} \approx k_d$  or  $k_{\text{off}} \ll k_d$ , i.e.  $\kappa_d \approx 1$  or  $\kappa_d \gg 1$ , target  
 298 coverage duration is comparable to or longer than the receptor life time. This can happen due  
 299 to: i) long period of target coverage; ii) fast receptor degradation; and iii) combination of both.  
 300 This might be biologically relevant when receptor homeostasis is tightly regulated at the  
 301 turnover level. The full model in (9) is used in this regime.

302 Again the eigenvalue method can be used to analyze the system dynamics. The  
 303 homogeneous part of (9) is  $\dot{\mathbf{X}} = \mathbf{A}\mathbf{X}$ . The trace of  $\mathbf{A}$  is  $T = \text{trace}(\mathbf{A}) = -(1 + \kappa_{\text{on}} + \kappa_d + \kappa_i)$ ,  
 304 the determinant of  $\mathbf{A}$  is  $\Delta = \det(\mathbf{A}) = \kappa_d + \kappa_{\text{on}}\kappa_i + \kappa_d\kappa_i$ . The two eigenvalues are

$$305 \lambda_{1,2} = \frac{1}{2} \left( T \mp \sqrt{T^2 - 4\Delta} \right).$$

306 For  $\lambda_1 = \frac{1}{2} \left( T - \sqrt{T^2 - 4\Delta} \right)$ , the associated eigenvector is

$$307 \mathbf{v}_1 = [v_{11} \quad v_{21}]^T = \left[ \frac{1 + \kappa_i - (\kappa_{\text{on}} + \kappa_d) - \sqrt{(1 + \kappa_i - \kappa_{\text{on}} - \kappa_d)^2 + 4\kappa_{\text{on}}}}{2\kappa_{\text{on}}} \quad 1 \right]^T.$$

308 For  $\lambda_2 = \frac{1}{2} \left( T + \sqrt{T^2 - 4\Delta} \right)$ , the associated eigenvector is

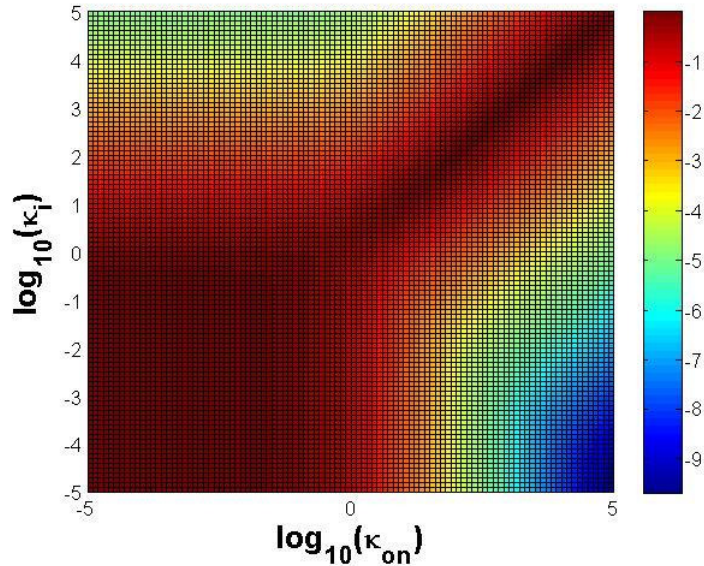
$$309 \mathbf{v}_2 = [v_{12} \quad v_{22}]^T = \left[ \frac{1 + \kappa_i - (\kappa_{\text{on}} + \kappa_d) + \sqrt{(1 + \kappa_i - \kappa_{\text{on}} - \kappa_d)^2 + 4\kappa_{\text{on}}}}{2\kappa_{\text{on}}} \quad 1 \right]^T.$$

310 Under the initial condition of  $\mathbf{X}_0 = [1 \ 0]^T$ , the general solution to the homogeneous part  
 311 can be written as  $\mathbf{M}(\tau)$  in (18). Taking the non-homogeneous part  $\mathbf{f} = [\kappa_d \ 0]^T$  into account,  
 312 the general solution to (9) is written as follows

$$313 \quad [r(\tau) \ c(\tau)]^T = \mathbf{M}(\tau)\mathbf{M}(0)^{-1}\mathbf{X}_0 + \mathbf{M}(\tau)\int_0^\tau \mathbf{M}(t)^{-1}\mathbf{f}(t)dt \quad (22)$$

314 The steady-state values of  $r$  and  $c$  can be obtained through numerical integration with (22), or  
 315 calculated explicitly by (10) and (11).

316 Similar to the heat map in Fig. 3, we first plot  $\log_{10}(\lambda_2 / \lambda_1)$  as a function of  $\kappa_{on}$  and  $\kappa_i$   
 317 in  $\log_{10}$  scales (Fig. 8). Taking  $k_{off} = k_d$ , i.e.  $\kappa_d = 1$  (Fig. 8 (a)), separation of time scales  
 318 happens if either  $k_{on} \gg k_{off}$  and  $k_i \ll k_{off}$  (blue region in Fig. 8 (a)), or  $k_{on} \ll k_{off}$  and  
 319  $k_i \gg k_{off}$  (light green region in Fig. 8 (a)), with the former leads to more pronounced effects.  
 320 In contrast, in the case of  $k_{off} = 0.001k_d$ , i.e.  $\kappa_d = 1000$  (Fig. 8 (b)), separation of time scales  
 321 takes place if  $k_i \ll k_{off}$  (bottom part in Fig. 8 (b)), and the condition of  $k_{on} \gg k_{off}$  makes the  
 322 separation more pronounced.

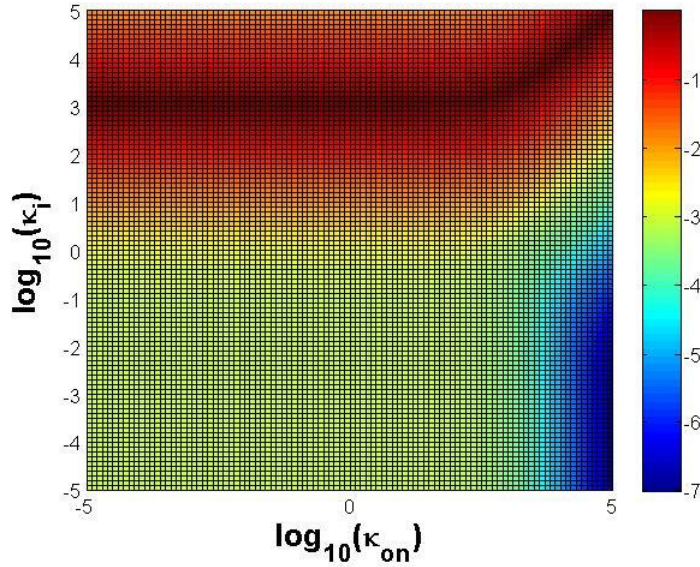


323

324

(a)  $k_{off} = k_d$





325

326

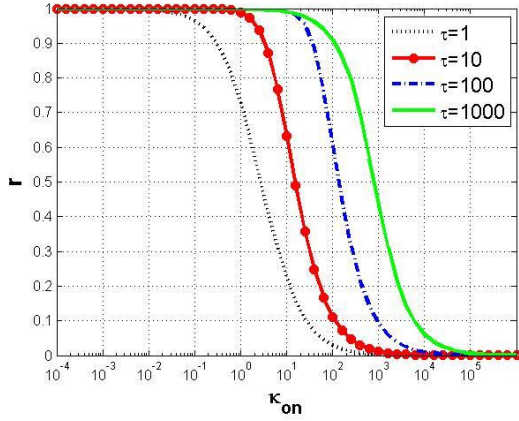
(b)  $k_{\text{off}} = 0.001k_d$

327 **Fig. 8**  $\log_{10}(\lambda_2 / \lambda_1)$  plotted as a function of  $\log_{10}(\kappa_{\text{on}})$  and  $\log_{10}(\kappa_i)$ . Values between -10  
 328 and 0 are colour-coded. (a)  $k_{\text{off}} = k_d$ ; (b)  $k_{\text{off}} = 0.001k_d$ .

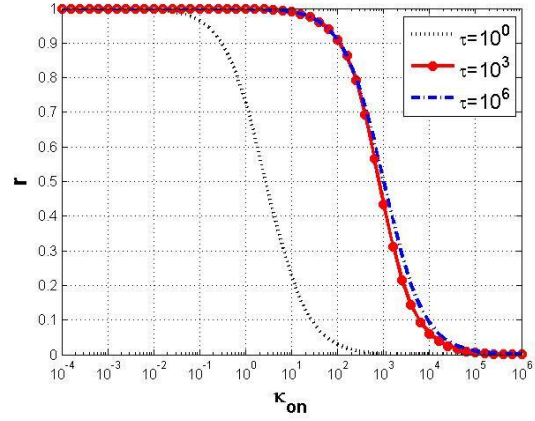
329 The following can be verified in this parametric regime:  $-v_{11}\lambda_2(\kappa_d + \lambda_1) < 0$ ,  
 330  $v_{12}\lambda_1(\kappa_d + \lambda_2) > 0$ . Considering the analytic solution, it is likely for  $r$  to decrease first with a  
 331 time scale determined by  $|\lambda_1|$  and then recover with a time scale determined by  $|\lambda_2|$  in the  
 332 longer term, if  $|\lambda_1|$  and  $|\lambda_2|$  are sufficiently apart.

333 An example is discussed to illustrate these ideas by taking  $k_{\text{off}} = k_d$  and  $k_i \ll k_d$ . This  
 334 means the receptor degradation is as fast as target coverage and the drug overcomes a large  
 335 energy barrier to covalently modify the receptor.

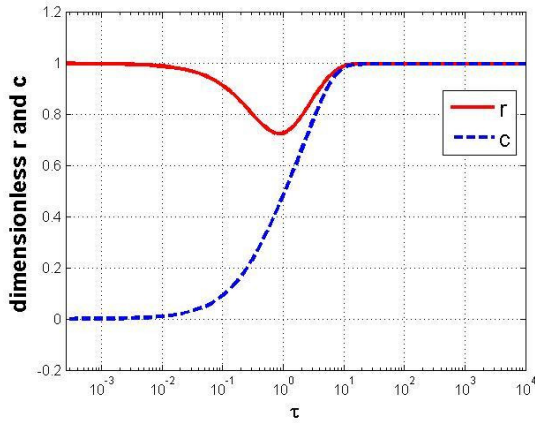
336 Suppose  $k_{\text{off}} = k_d$  and  $k_i = 0.001k_d$ . Under this condition, receptor initially decreases as a  
 337 result of drug inhibition, and then recovers towards steady states (see Fig. 9 (c) and Fig. 9 (d)).  
 338 In the context of dose response curves, this means measurement taken before recovery in  $r$   
 339 would make the drug appear more potent than the actual steady-state response. For  $\kappa_{\text{on}} = 1$ ,  $r$   
 340 is predicted to be smaller for  $\tau = 1$  than for  $\tau = 10, 100, 1000$  (Fig. 9 (a)). In addition, this  
 341 trend is consistent throughout  $\kappa_{\text{on}}$  values to a larger range (Fig. 9 (b)). Hence, the dose  
 342 response simulated for  $\tau = 1$  (black dotted curve) appears to be more potent than any other  
 343 curves in Fig. 9 (a)-(b).



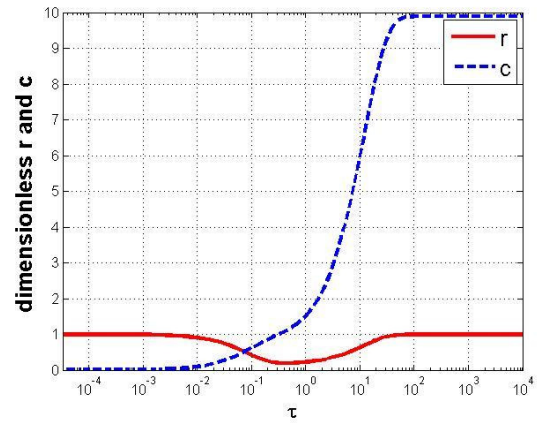
(a)  $\tau = [1, 10^3]$



(b)  $\tau = [1, 10^6]$



(c)  $\kappa_{on} = \kappa_d = 1$



(d)  $\kappa_{on} = 10, \kappa_d = 1$

**Fig. 9** Dose response curves, time response of  $r$  and  $c$  under  $\kappa_i = 0.001$ .

According to the heat map in Fig. 8 (a), higher  $\kappa_{on}$  leads to smaller  $\lambda_2$  (the blue region in Fig. 8 (a)), which makes recovery time in  $r$  being longer. To examine this observation, time responses of  $r$  and  $c$  are simulated for  $\kappa_{on} = 1$  and  $\kappa_{on} = 10$ , respectively, as shown in Fig. 9 (c) and (d). It can be seen that time response simulation at  $\kappa_{on} = 10$  predicts an elongated recovery period in  $r$  (Fig. 9 (d)) compared with that in  $\kappa_{on} = 1$  (Fig. 9 (c)). This observation is consistent with the separation of different dose response curves in Fig. 9 (a).

In slow drug process, the increase of complex concentration is monotonic over time, while the receptor concentration first decreases in a short time and then increase towards a constant level in a longer time. The numerical solutions for  $r$  and  $c$  at steady states shown in Fig. 9 (c) and (d) are validated by the model-based analytical results in (10) and (11).

360 **5 Applications**

361 Aberrant activity in Epidermal Growth Factor Receptor (EGFR) signaling has profound  
 362 implications in different types of tumour. Recently,  $k_{\text{off}}/k_{\text{on}}$  and  $k_i$  are reliably quantified  
 363 from cell-free assays for different irreversible EGFR mutant (EGFRm) inhibitors [20].  
 364 However, this study was not able to determine the actual values of  $\kappa_{\text{on}} = k_{\text{on}}^* [\text{afatinib}]/k_{\text{off}}$   
 365 and  $k_{\text{off}}$ . Instead,  $k_{\text{on}}^*$ , that is  $k_{\text{on}}/[\text{drug}]$  in our context, was assumed to be close to diffusion  
 366 limit at  $100\mu\text{M}^{-1}\text{s}^{-1}$  in order to calculate values for  $k_{\text{off}}$ . The reported values are tabulated  
 367 below:

compound	$k_{\text{off}}, \text{s}^{-1}$	$k_i, \text{s}^{-1}$	Ki(nM)
CI-1033	0.19±0.04	0.011±0.0002	1.9±0.4
dacomitinib	1.1±0.1	0.0018±0.0001	10.7±0.9
afatinib	0.3±0.1	0.0024±0.0003	2.8±0.6
neratinib	0.2±0.1	0.0011±0.0002	2.4±0.5
CL-387785	18±4	0.002±0.0003	180±40
WZ-4002	23±5	0.0049±0.0015	230±50

368 Table 1. Parameter values inferred from reaction progress curves measured for H1975 cells  
 369 carrying L858R and T790M mutations in EGFR, using an ODE model. This table is  
 370 reproduced from the supplementary information in [20]. The plus-or-minus values are  
 371 standard deviations from averaging three replicated, entirely independent experiments.

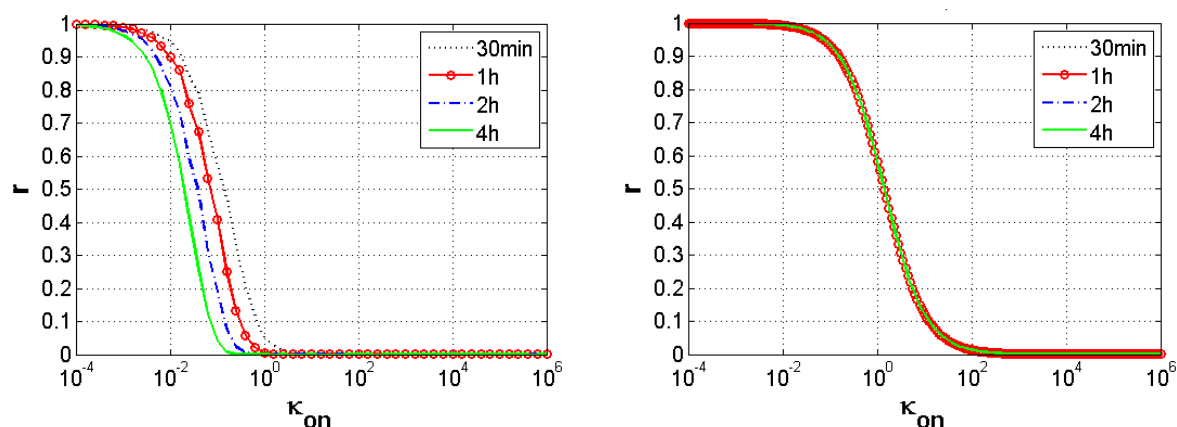
372  $K_i = k_{\text{on}}/k_{\text{off}}$ .

373 We simulated the cell-free assay of afatinib by using the model in (9) by taking  $\kappa_d = 0$ . This  
 374 predicts the  $\text{IC}_{50}$  for  $\kappa_{\text{on}}$  at 30-minutes incubation has a mean value of 0.13 (i.e. assuming  
 375  $k_i = 2.4 \times 10^{-3} \text{s}^{-1}$ ,  $k_{\text{off}} = 0.3 \text{s}^{-1}$ ) (see Fig. 10 (a)). Since  $\kappa_{\text{on}} = k_{\text{on}}^* [\text{afatinib}]/k_{\text{off}}$ , afatinib's  
 376  $\text{IC}_{50}$  at 30-minutes incubation is predicted to be 0.4nM. Considering different combinations  
 377 of  $k_i$  and  $k_{\text{off}}$  values as reported in Table 1, afatinib's  $\text{IC}_{50}$  at 30-minute incubation is  
 378 predicted to be within the range of [0.27,0.6] nM.

379 It is reported that the internalisation rate of EGFR receptor is approximately  $0.2\text{min}^{-1}$  in  
 380 breast cancer cells [21]. Hence,  $\kappa_d = k_d/k_{\text{off}} = 1.1 \times 10^{-2}$ . Considering  $\kappa_i = 8.0 \times 10^{-3}$ , this is  
 381 similar to the fast drug process parametric regime discussed in Section 3.3. Model simulation  
 382 in Fig. 6 suggests dose response curves taken at  $\tau = 1$  and  $\tau = 100$  should be close.

383 Using model (12) to mimic in vitro cell assay conditions by taking  $\kappa_d = 1.1 \times 10^{-2}$ , simulated  
 384 dose response curves at different incubation durations shift further to right (Fig. 10 (b))  
 385 compared with that of  $\kappa_d = 0$  (Fig. 10 (a)). In Fig. 10 (b), with  $\text{IC}_{50}$  for  $\kappa_{\text{on}}$  at 1-hour  
 386 incubation at approximately 1.4, a 10-fold increase from the predicted protein-based assay  
 387 (i.e. 0.13) is observed. Consistent with these simulation results, approximately 10-fold  
 388 difference was reported for cell-based assay and protein-based assay for afatinib [21]

389 It can be seen from the above discussions that the simple model in (9) can be used  
 390 conveniently to generate insights into the connections and differences between protein-based  
 391 assay and cell-based assay.



392

393 (a)  $\kappa_d = 0$ ,  $\kappa_i = 8.0 \times 10^{-3}$ . This mimics  
 394 the cell-free assay condition.

(b)  $\kappa_d = 1.1 \times 10^{-2}$ ,  $\kappa_i = 8.0 \times 10^{-3}$ . This  
 mimics the in vitro cell assay.

395 **Fig. 10** Simulated dose response curves for afatinib.

## 396 6. Conclusions and discussions

397 At lead generation and optimization, it is important to understand the Mechanism Of  
 398 Action (MOA) of a chemical compound, as well as the Structure-Activity Relationship  
 399 (SAR), in the hope that ultimately a compound with sufficient therapeutic efficacy is taken  
 400 further for preclinical development. Reversibility of a compound is a crucial aspect of MOA

401 characterisation. This often remains unknown for compounds coming out of empirical  
402 screening methods. Towards this goal, assays have been established to study inhibition  
403 reversibility [22]. It is generally accepted that response to irreversible inhibitors are time-  
404 dependent. Hence, it is often taken for granted that time-independence indicates inhibition  
405 reversibility. However, our model-based analysis refutes this claim.

406 We demonstrated iff inhibitor binding and dissociation processes are much quicker than  
407 receptor turnover, this system can be approximated by one concerning inhibition only, which  
408 is equivalent to the protein-based assay. Based on the numerical simulation using a simple  
409 model, it is observed that for protein-based assays, under certain parameter conditions, the  
410 dose response curves can be very similar to each other (compare the middle curves in Fig. 2  
411 (d)), given 1000-fold variation in incubation time. This indicates dose responses might appear  
412 time-invariant for a particular parameter setting. In practice, these data might not be  
413 statistically different and can be erroneously taken as evidence of reversible inhibitor.

414 We subsequently analyzed the impact of cell parameters on dose response, including target  
415 synthesis and degradation, using the proposed model. Our ensuing analysis of the eigenvalues  
416 provides a more general understanding. For dose response to appear time-invariant, the  
417 apparent first-order association rate  $\kappa_{on}$  and the first-order covalent bond formation rate  $\kappa_i$   
418 need to be well separated so that the system has two very different time scales. In particular,  
419 when a slowly-dissociating irreversible drug is applied to a receptor under fast turnover, dose  
420 response may be highly similar to each other under a variety of incubation periods. Hence, it  
421 is inappropriate to conclude an inhibitor being reversible given time-independent dose  
422 response, either based on protein-based assay or cell-based assay.

423 The main purpose of this analysis is to demonstrate the relationship between dose response  
424 and parameter values in drug and cell processes. For the sake of simplicity, we only  
425 considered a linear model in which each reaction follows first-order kinetics. In addition, we  
426 did not consider biological regulation over synthesis, degradation and sub-cellular  
427 localisation of a receptor [20]. Results obtained in this paper are specific to the form of this  
428 linear model. In reality, receptors are often regulated under different levels via feedback  
429 mechanisms. This often necessitates mechanistic modelling of a biological pathway to aid in  
430 interpretation of in vitro cell assays.

431 It is evident from both numerical simulation and analytical study that the proposed model  
432 is globally asymptotically stable. For the fast drug process considering complex elimination,

433 the reduced model (12) is proposed. The receptor concentration decreases monotonically to  
434 its steady-state level of zero, while the complex concentration initially increases rapidly and  
435 then decreases gradually to zero when the complex elimination is considered (see (13) for  
436 steady-state calculation). When the complex elimination is negligible, the reduced model (19)  
437 is used. The system will have non-zero steady states for both  $r$  and  $c$  following a conservation  
438 law of  $r_{ss} + c_{ss} = 1$  (see (21) for the explicit solution). For the slow drug process including  
439 both reactions (1) and (2), the full model (9) is used to describe the dynamic system, and the  
440 steady-states are explicitly represented by (10) and (11) for  $r$  and  $c$ , respectively. In this case,  
441 the complex concentration increases monotonically over the whole process, but the receptor  
442 concentration first decreases rapidly and then increases gradually on a slower time scale back  
443 towards its steady state. The similar rebound behaviour in receptor was also observed and  
444 discussed in other TMDD model-based studies [12; 14; 15].

445 For a drug discovery and development programme, the in vitro model should be used to  
446 identify parameter values from in vitro data. These parameters can be used subsequently to  
447 help identify the remaining parameter values in the in vivo model. This step-wise fitting may  
448 reduce uncertainty in parameter estimation. In this context, the in vitro model described in  
449 this paper improves the utility of TMDD models.

## 450 **Acknowledgment**

451 TY would gratefully acknowledge Hitesh Mistry (University of Manchester), James Yates  
452 (AstraZeneca UK Ltd) and Chris Brackley (University of Edinburgh) for useful discussions.  
453 HY would like to thank Professor Peter Halling and Mr Hui Yu from the University of  
454 Strathclyde for useful discussions and support in Matlab coding.

## 455 **References**

- 456 [1] Sorger, P. K., Allerheiligen, S. R., Abernethy, D. R., et al.: 'Quantitative and systems  
457 pharmacology in the post-genomic era: new approaches to discovering drugs and  
458 understanding therapeutic mechanisms', NIH Bethesda, An NIH white paper by the  
459 QSP workshop group, 2011), 1-48
- 460 [2] Gibiansky, L. and Gibiansky, E.: 'Target-mediated drug disposition model:  
461 approximations, identifiability of model parameters and applications to the population  
462 pharmacokinetic and pharmacodynamic modeling of biologics', Expert Opin Drug  
463 Metab Toxicol, 2009, **5**, (7), 803-812

- 464 [3] Ma, P.: 'Theoretical considerations of target-mediated drug disposition models:  
465 simplifications and approximations', *Pharmaceutical research*, 2012, **29**, (3), 866-882
- 466 [4] Marathe, A., Krzyzanski, W. and Mager, D. E.: 'Numerical validation and properties of a  
467 rapid binding approximation of a target-mediated drug disposition pharmacokinetic  
468 model', *Journal of Pharmacokinetics and Pharmacodynamics*, 2009, **36**, (3), 199-219
- 469 [5] Yan, X., Mager, D. E. and Krzyzanski, W.: 'Selection between Michaelis–Menten and  
470 target-mediated drug disposition pharmacokinetic models', *Journal of pharmacokinetics  
471 and pharmacodynamics*, 2010, **37**, (1), 25-47
- 472 [6] Vicini, P.: 'Multiscale modeling in drug discovery and development: future opportunities  
473 and present challenges', *Clinical Pharmacology & Therapeutics*, 2010, **88**, (1), 126-129
- 474 [7] Mager, D. E. and Krzyzanski, W.: 'Quasi-equilibrium pharmacokinetic model for drugs  
475 exhibiting target-mediated drug disposition', *Pharmaceutical Research*, 2005, **22**, (10),  
476 1589-1596
- 477 [8] Gibiansky, L. and Gibiansky, E.: 'Target-mediated drug disposition model: relationships  
478 with indirect response models and application to population PK–PD analysis', *Journal  
479 of Pharmacokinetics and Pharmacodynamics*, 2009, **36**, (4), 341-351
- 480 [9] Orrell, D. and Fernandez, E.: 'Using predictive mathematical models to optimise the  
481 scheduling of anti-cancer drugs', *Innovations in Pharmaceutical Technology*, 2010, **33**,  
482 58-62
- 483 [10] Yankeelov, T. E., Atuegwu, N., Hormuth, D., et al.: 'Clinically relevant modeling of  
484 tumor growth and treatment response', *Science Translational Medicine*, 2013, **5**, (187),  
485 187ps9-187ps9
- 486 [11] Bonate, P.: 'What happened to the modeling and simulation revolution?', *Clinical  
487 Pharmacology & Therapeutics*, 2014, **96**, (4), 416-417
- 488 [12] Aston, P. J., Derks, G., Agoram, B. M. and Van Der Graaf, P. H.: 'A mathematical  
489 analysis of rebound in a target-mediated drug disposition model: I. Without feedback',  
490 *Journal of Mathematical Biology*, 2014, **68**, (6), 1453-1478
- 491 [13] Peletier, L. A. and Gabrielsson, J.: 'Dynamics of target-mediated drug disposition',  
492 *European Journal of Pharmaceutical Sciences*, 2009, **38**, (5), 445-464
- 493 [14] Peletier, L. A. and Gabrielsson, J.: 'Dynamics of target-mediated drug disposition:  
494 characteristic profiles and parameter identification', *Journal of Pharmacokinetics and  
495 Pharmacodynamics*, 2012, **39**, (5), 429-451
- 496 [15] Aston, P. J., Derks, G., Raji, A., Agoram, B. M. and Van Der Graaf, P. H.:  
497 'Mathematical analysis of the pharmacokinetic–pharmacodynamic (PKPD) behaviour

498 of monoclonal antibodies: predicting in vivo potency', *Journal of theoretical biology*,  
499 2011, **281**, (1), 113-121

500 [16] Strelow, J., Dewe, W., Iversen, P., et al.: 'Mechanism of Action assays for Enzymes',  
501 2004,

502 [17] Nagar, S., Jones, J. P. and Korzekwa, K.: 'A numerical method for analysis of in vitro  
503 time-dependent inhibition aata. Part 1. theoretical considerations', *Drug Metabolism  
504 and Disposition*, 2014, **42**, (9), 1575-1586

505 [18] Copeland, R. A., Pompliano, D. L. and Meek, T. D.: 'Drug–target residence time and its  
506 implications for lead optimization', *Nature Reviews Drug Discovery*, 2006, **5**, (9), 730-  
507 739

508 [19] You, T., Stansfield, I., Romano, M. C., Brown, A. J. and Coghill, G. M.: 'Analysing  
509 GCN4 translational control in yeast by stochastic chemical kinetics modelling and  
510 simulation', *BMC systems biology*, 2011, **5**, (1), 131

511 [20] Lauffenburger, D. A. and Linderman, J. J. *Receptors: models for binding, trafficking,  
512 and signaling*. Oxford University Press New York:, 1993.

513 [21] Hendriks, B. S., Opresko, L. K., Wiley, H. S. and Lauffenburger, D.: 'Coregulation of  
514 Epidermal Growth Factor Receptor/Human Epidermal Growth Factor Receptor 2  
515 (HER2) Levels and Locations Quantitative Analysis of HER2 Overexpression Effects',  
516 *Cancer Research*, 2003, **63**, (5), 1130-1137

517 [22] Schwartz, P. A., Kuzmic, P., Solowiej, J., et al.: 'Covalent EGFR inhibitor analysis  
518 reveals importance of reversible interactions to potency and mechanisms of drug  
519 resistance', *Proceedings of the National Academy of Sciences*, 2014, **111**, (1), 173-178  
520